

INVESTIGATION ON THE ANTI-PENETRATION PERFORMANCE OF UD – A THREE-DIMENSIONAL ORTHOGONAL WOVEN FABRIC COMPOSITE REINFORCED STRUCTURE

CHAOMING SHEN, YANG CHEN

School of Naval Architecture and Ocean Engineering, Jiangsu University of Science and Technology, Zhenjiang, China

LEI LIU

*School of Naval Architecture and Ocean Engineering, Jiangsu University of Science and Technology, Zhenjiang, China;
and China Merchants Jinling Shipyard (Yangzhou) Dingheng Co., Ltd., Yangzhou, China*

ZEXIN ZHANG

School of Naval Architecture and Ocean Engineering, Jiangsu University of Science and Technology, Zhenjiang, China

BAIJIAN TANG

*School of Naval Architecture and Ocean Engineering, Jiangsu University of Science and Technology, Zhenjiang, China;
and School of Civil Engineering, Suzhou University of Science and Technology, Suzhou, China*

FUSHAN LI

China Special Equipment Inspection and Research Institute, Jiaxing, China

DENGHUI QIAN

*School of Naval Architecture and Ocean Engineering, Jiangsu University of Science and Technology, Zhenjiang, China
e-mail: dhqian@just.edu.cn*

A uni-direction (UD) laminate and three-dimensional (3D) orthogonal woven fabric made of ultra high molecular weight polyethylene (UHMWPE) are used as main reinforced units combined with aluminum alloy plates to form a reinforced sandwich structure. Penetration tests are carried out on four composite reinforced structures with different structure forms by a 7.62 mm steel core projectile. The target plate size is 150 mm×150 mm. Besides, Ansys/LS-Dyna software is applied to simulate the penetration process, and the simulation results are in good agreement with the test results. All the results demonstrate that with the same total thickness of UD laminates, 20 mm UD laminates have better penetration resistance than four 5 mm UD laminates. The less the number of UD laminates, the better anti-penetration performance of the overall structure. The 3D orthogonal woven fabric has the advantage of spatial integrity, which can effectively restrain deformation of laminates and absorb energy behind UD laminates, so as to obtain better anti-penetration performance. In the core structure with a total thickness of 28 mm, when the thickness ratio of 3D orthogonal woven fabric is between 30% and 35%, the protection ability and lightweight requirements of the sandwich structure can be better considered.

Keywords: three-dimensional orthogonal woven fabric, anti-penetration performance, ultra high molecular weight polyethylene, thickness ratio

1. Introduction

The UD laminate made of UHMWPE fiber, which has characteristics of high specific strength, high specific modulus, excellent impact resistance and so on, is one of the most widely used bulletproof materials in the world. Since the material can transmit stress wave and dissipate impact kinetic energy faster, it has excellent anti-penetration performance. However, the damage

area is large and the interlayer is easily stratified if the UD laminate is impacted, which is not conducive to the resistance of the second impact.

Compared with the fiber laminate used for a spatial integral weaving material, the 3D fabric composite material has greater interlaminar strength and ability to resist lamination damage (Xiong *et al.*, 2018). It is an effective way to improve the anti-penetration performance of the protective structure to compose the 3D fabric composite plate by filling the internal pores with the energy absorbing material. Presently, different 3D fabrics have been researched and applied in aerospace and other protective engineering fields (Liang and Fang, 2014). 3D woven fabric structures are shown in Fig. 1.

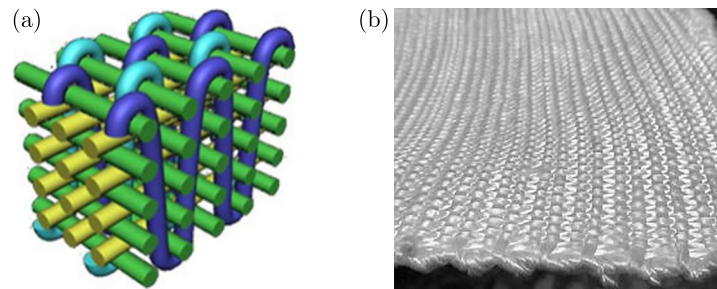


Fig. 1. Structure of the 3D woven fabric: (a) 3D model, (b) physical photo

Penetration tests and numerical simulations are the main methods to study the impact resistance and failure mechanism of 3D fabric composites. Hu *et al.* (2021), Song *et al.* (2020) and Wu *et al.* (2019) analyzed failure modes of several 3D fabrics under the high-speed or low-speed impact, and explored their failure mechanism and energy absorption characteristics. Deng *et al.* (2018) studied penetration resistance characteristics of rigid ogival-nosed projectiles on braided composite laminated plates, and studied the influence law of the impact angle of the projectile body on its ballistic limit. They found that when the impact angle of the projectile body is 45° , the ballistic limit of the target plate was the highest, followed by 0° , and the ballistic limit was the lowest when the impact angle was 30° . Walter *et al.* (2009) explored failure forms of 3D braided fiberglass reinforced composite plates under small caliber projectiles, and found that the main failure mode was laminar failure of the braided surface. By adding yarn in the Z -axis direction of the fiber cloth, laminar failure of fiberglass reinforced composite plates could be limited and the anti-penetration performance could be improved. Tan *et al.* (2018) established a macro-continuum damage finite element model for 3D four-direction braid composites, and found that the calculated residual velocity and experimental error of the model were within 5%, thus verifying the effectiveness of the macro-finite element model. Sun *et al.* (2009) analyzed ballistic impact results of 3D orthogonal woven composites by using a macroscopic finite element model, and found that the results were basically consistent with the experimental results.

In this paper, the UHMWPE 3D orthogonal woven fabric composite plate is added to the aluminum alloy – the UD laminate sandwich structure. Penetration tests and numerical simulations on fabric reinforced composite structures with different structure forms are carried out to explore the anti-penetration performance of the fiber composite structure with the UHMWPE 3D orthogonal woven fabric.

2. Design of penetration test scheme

2.1. Design and preparation of composite reinforced structure target plates

Due to weak anti-ultraviolet aging ability of polymer materials, which is not conducive to connection with existing fabrics, the use of aluminum panels and backplanes can effectively solve

these problems. 7075-T6 aluminum alloy is a cold-treated forged alloy with high strength and provides the highest ballistic resistance, so the front and rear panels of the composite target plates are made of 7075 light and high strength aluminum alloy plates with thickness of 1 mm, 3 mm and 5 mm, respectively. The dimensions are 150 mm×150 mm. The UD laminates are made of the UHMWPE fiber which is tiled and hot-pressed in the manner of 0°-90°. The yarn size is 400D and material density is 0.98 g/cm³. The thicknesses of UD laminates are 5 mm and 20 mm. The dimensions are 150 mm×150 mm. The 3D fabric composite plate is molded by filling the resin matrix of bisphenol A into the 3D orthogonal woven fabric preform. Since the injected bisphenol resin has good fluidity and can freely penetrate into the fiber, all target plates are pressed and solidified by heavy objects to ensure stable solidification of the interface between the materials. After forming, a magnifying glass is used to observe defects at the joint to avoid the influence of quality defects on the experimental results. The areal density of the processed 3D fabric composite plate is 0.94 g/cm² and the thickness is 8 mm. The dimensions are 150 mm×150 mm. The plane dimensions of composite target plates are 150 mm×150 mm, and the total areal density is about 44 kg/m².

In the case of the same total surface density, using the same basic material, through different arrangements to find the optimal structure, we design four different structural forms as shown in Fig. 2. In the figure, V_0 is the initial impact velocity. The thicknesses of the front and rear panels of structure I and II are 1 mm and 5 mm. The thicknesses of the front and rear panels of structure III and IV are 3 mm. The plates are bonded after mixing with the epoxy AB adhesive resin.

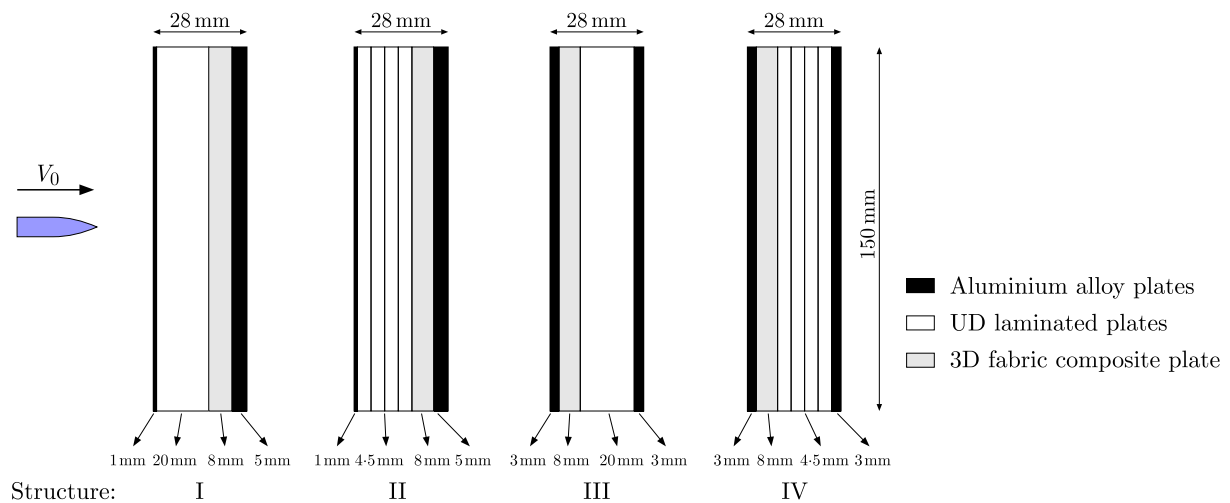


Fig. 2. Schematic of composite target plates

2.2. Test device

The test projectile body is a 7.62 mm steel core projectile. The actual diameter of the warhead is 7.92 mm and the mass is about 8.4 g. The size and shape of the projectile body are shown in Fig. 3.

The main equipment of the penetration test includes a ballistic gun, gun holding device, high-speed image recording system, calibrated plate, target plate clamping device and projectile recovery device. The high-speed camera is placed on the side of the clamping device of the target plate and facing the calibrated plate. The velocity of the projectile is calculated mainly by processing the image of the high-speed camera. The layout of the penetration device and the test site are shown in Fig. 4.

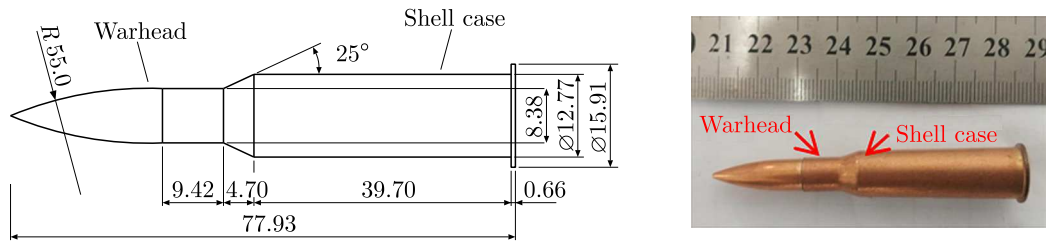


Fig. 3. Size and shape of the projectile (unit: mm)

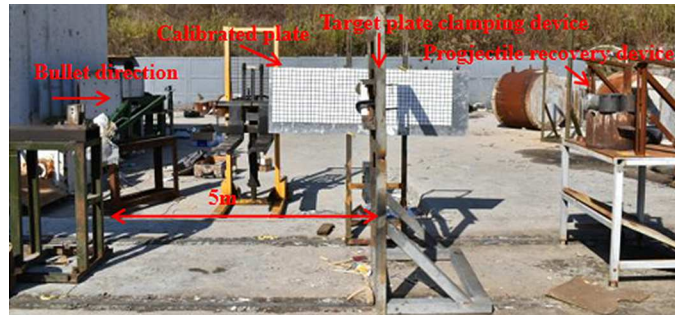
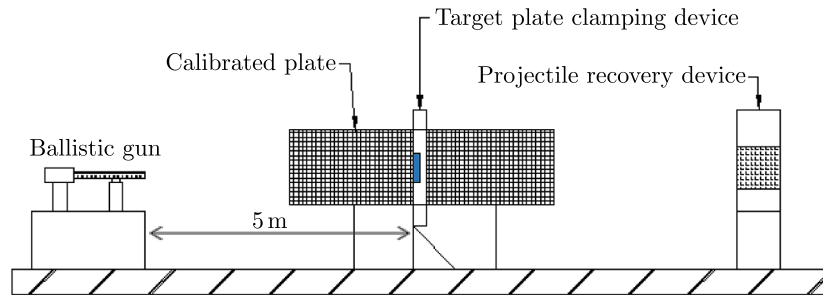


Fig. 4. Layout of the penetration device and test site

3. Test results

The ballistic test results are listed in Table 1, and the valid data are obtained from each of the four tests. The range of projectile incident velocity is 855.48 m/s to 861.71 m/s, STDEV is 2.79, so it can be considered that the incidence velocity is basically the same, where the residual velocity is 0, indicating that the projectile does not penetrate the composite target plate.

Table 1. Ballistic test results

Structure of target plates	Incident velocity [m/s]	Residual velocity [m/s]	Degree of breakage of backplane
I	861.71	0	not penetrated, cracked, slightly uplifted
II	859.63	286.14	penetrated, large area of cataclastic damage
III	855.48	0	not penetrated, cracked, uplift about 32 mm
IV	856.81	412.91	penetrated, cataclastic damage, uplift about 25 mm

3.1. Failure patterns of the panel

The failure patterns of the front panel after being penetrated by the projectile are shown in Fig. 5. The front panel can be observed with obvious shear and chisel marks, which makes

two failure patterns generate: I and II are circular holes which are directly penetrated and accompanied by cracks; III and IV are outward curled petal-like holes of aluminum alloy at the edge of bullet holes. The reason for this phenomenon is that the 3 mm aluminum alloy plate is thick, so it has the ability to produce enough plastic deformation under the condition of the impact of the projectile body. The diameters of all bullet holes did not differ much, being about 9 mm.

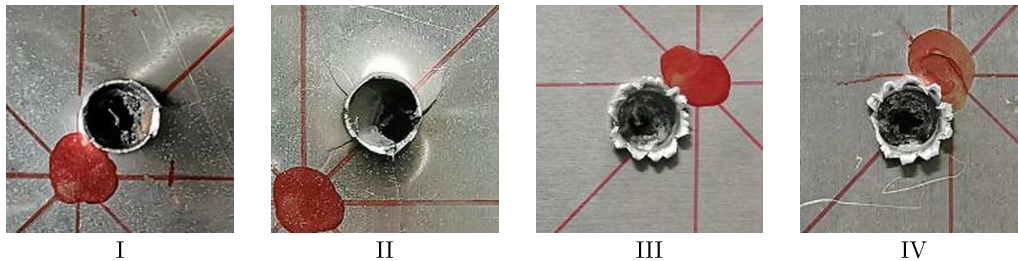


Fig. 5. Failure patterns of the front panel of composite target plates

The failure patterns of the rear panel of the composite target plates are shown in Fig. 6. It can be seen from the figure that the failure patterns of the rear panel are completely different. From the perspective of penetrating and non-penetrating, the failure patterns can be roughly divided into uplift and radial crack (I, III) and cataclastic failure (II, IV). Further speaking, although structure III is not penetrated, the maximum amplitude of uplift is 32 mm and accompanied by multiple cracks; structure II is penetrated and the maximum breakage range is 45 mm×53 mm; The breakage condition of structure IV is between the former two, the height of uplift is 25 mm and the diameter of the hole is about 11 mm. Not only structure I is not penetrated, but also the uplift amplitude is the lowest, and there is only one crack. Therefore, it can be considered that the anti-penetration performance of structure I is better than in the other three structures.

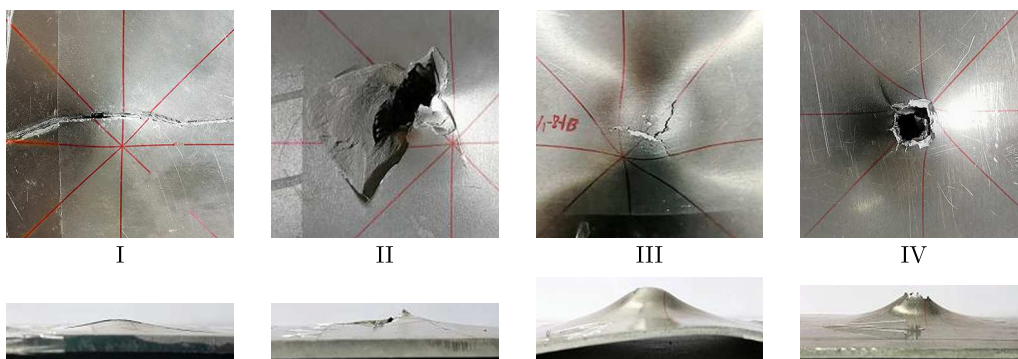


Fig. 6. Failure patterns of the rear panel of composite target plates

3.2. Failure patterns of the core layer

In order to observe deformation and breakage of the 3D fabric composite plate and its effect on the composite target plates, the cemented aluminum alloy plates are disassembled from the core layer after the test. Figure 7 shows the failure morphology of the core layer facing the surface, internal surface and back surface of each structure. Figure 8 shows the failure side view of the core layer of each structure.

In Figs. 7a and 7b, when the projectile body impacts the polyethylene plate at high speed, the target plate exhibits adiabatic shear failure. Local high temperature is generated in the shear band, which leads to fiber fusing in the penetration zone, and the outer matrix is scorched and

some black substances are produced. Structure I projectile body does not penetrate even the laminated plates, and a small amount of deformation occurs in the 3D fabric plate. Structure II is penetrated and a small number of fiber bundles are observed to be damaged and surround the bullet holes in the 3D fabric plate. According to Figs. 7c and 7d, the high temperature generated by the projectile body after penetrating the 3D fabric plate and impacting the laminates will make the internal holes gradually become bigger, but the shape of the breach does not change greatly.

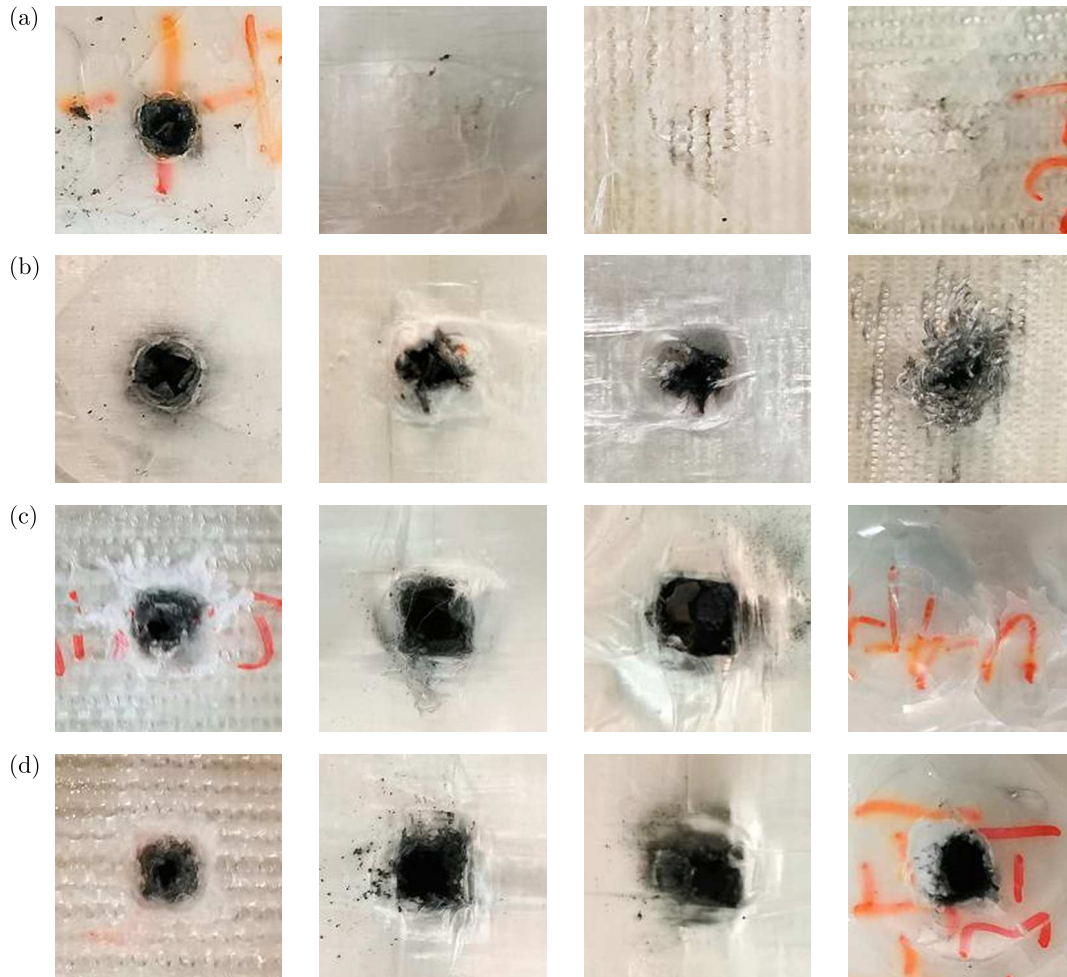


Fig. 7. Failure morphology of the core layer of each structure: (a) structure I, (b) structure II, (c) structure III, (d) structure IV

In Fig. 8, different degrees of delamination occur in each laminated plate, and the structure with four laminated plates is more serious. The factor of whether structure I and II, III and IV are penetrated is the number of laminated plates. Therefore, it can be considered that the less the number of laminated plates with the same total thickness, the better anti-penetration performance of the composite reinforced structure.



Fig. 8. Failure side view of each structure core layer

Based on Figs. 6, 7 and 8, it is found that when the 3D fabric plate is placed in front of the laminated plate, the projectile body quickly penetrates the 3D fabric plate and impacts the rear laminated plates, resulting in a large deflection deformation of the laminated plates and driving the back plate to the arch back. When the 3D fabric is placed behind the laminate and the projectile body impacts the front laminate, the 3D fabric plate can resist the deformation of the laminates to a large extent and absorb a large amount of energy due to the integrity of the space. Therefore, it can be considered that the anti-penetration performance of the composite reinforced structure is better when the 3D fabric plate is placed behind the laminated plates.

4. Numerical simulation of the penetration response of the target plate

4.1. Numerical simulation model

Since the UHMWPE fiberboard is made of hot pressing in the way of 0° - 90° , and the thickness of each layer is about 0.168 mm, the modeling in accordance with this thickness will require very high hardware conditions and cause unacceptable time cost. In order to give consideration to calculation accuracy and efficiency, a macro equivalent modeling is adopted. The idea of the macro equivalent modeling is to model the fiber and matrix as a whole. This paper uses ANSYS/LS-DYNA software to carry out the macro modeling of composite target plates in the test. In order to simulate the layered effect of laminates, it is assumed that 2 mm in the thickness direction is a more appropriate layer. Considering the symmetry between the projectile and the target plate as well as reducing the amount of calculation, this paper establishes a 1/4 model and sets symmetry constraints on the symmetry plane and fixed constraints around the target plate.

The projectile model and the center area impacted of the target plate model are mesh-refined, and the size length is 0.5 mm. Face erosion contact is arranged between the projectile body and the target plate, and face automatic contact with fixed connection is arranged between layers. Taking structure I as an example, the projectile body and target plate after grid division are shown in Fig. 9.

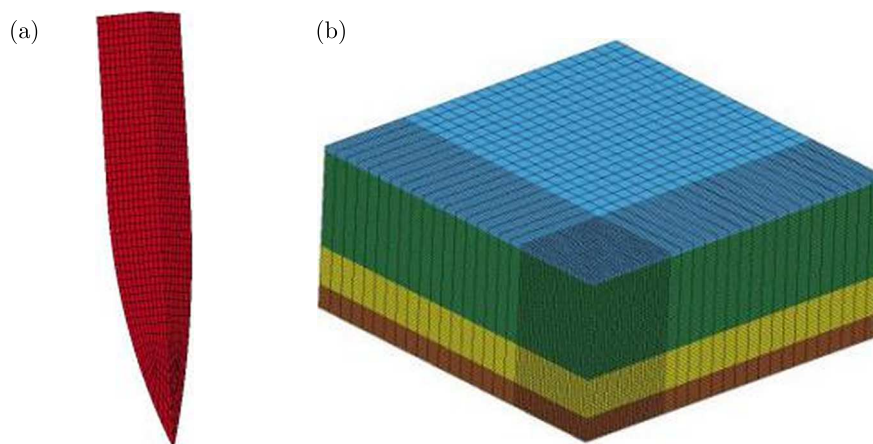


Fig. 9. Numerical simulation model of structure I: (a) projectile body, (b) target plate of structure I

4.2. Material model

4.2.1. Constitutive model of the projectile body and aluminum alloy

The model of the projectile body does not consider the copper coating on the actual projectile surface, and its interior is high strength tool steel. The composite target panel is made of 7075

aluminum alloy as described above. Johnson and Cook's (1983) model is used for both metal material models, and the equation is shown in Eq. (4.1). The corresponding Johnson-Cook damage (You-Zhi *et al.*, 2008) model is shown in Eq. (4.2). The material parameters of the projectile body and aluminum alloy (Liu, 2020; Chen *et al.*, 2019) are shown in Table 2

$$\sigma_y = (A + B\bar{\varepsilon}^{n'}) (1 + C \ln \varepsilon^*) \left[1 - \left(\frac{T - T_r}{T_m - T_r} \right)^m \right] \quad (4.1)$$

where σ_y is the equivalent stress, A , B , C , n and m are material constants, $\bar{\varepsilon}^p$ is effective plastic strain, $\varepsilon^* = \dot{\varepsilon}^p / \dot{\varepsilon}_0$ is dimensionless plastic strain rate, T is temperature, T_r is indoor temperature, and T_m is the melting point of the material

$$\varepsilon^f = (D_1 + D_2 \exp D_3 \sigma^*) (1 + D_4 \ln \varepsilon^*) (1 + D_5 T^*) \quad (4.2)$$

where D_1 - D_5 are fracture parameters of materials.

Table 2. Constitutive and damage parameters of the projectile and aluminum alloy

Material parameters	Projectile	Aluminum alloy	Material parameters	Projectile	Aluminum alloy
ρ [kg/m ³]	7830	2700	m	1.61	1.015
G [GPa]	0.77	0.27	$\dot{\varepsilon}_0$	$0.1 \cdot 10^{-5}$	$2.1 \cdot 10^{-3}$
T_r [K]	293	293	D_1	5.00	0.209
T_m [K]	1795	910	D_2	0.00	2.426
A [MPa]	792	547	D_3	0.00	-7.989
B [MPa]	510	687	D_4	0.00	0.036
n	0.26	0.740	D_5	0.00	0.697
C	0.014	0.017			

4.2.2. UHMWPE laminates and the 3D fabric constitutive model

This paper adopted MAT_COMPOSITE_DAMAGE (MAT_22) statement in LS-DAYNA for UHMWPE fiberboard. Mat_022 model characterizes orthotropic composite materials with optional brittle failure criteria following the failure model proposed by Qu *et al.* (2020), see Table 3 for related material parameters.

Table 3. Material parameters of UD laminates

ρ [g/cm ³]	E_1 [GPa]	E_2 [GPa]	E_3 [GPa]	ν_{12} [-]	ν_{13} [-]	ν_{23} [-]	G_{12} [GPa]	G_{13} [GPa]
0.98	30.7	30.7	1.97	0.008	0.044	0.044	0.73	0.67
G_{23} [GPa]	H_{fail} [GPa]	S_c [GPa]	X_t [GPa]	Y_t [GPa]	Y_c [GPa]	S_n [GPa]	S_{yz} [GPa]	S_{xz} [GPa]
0.67	2.2	0.36	3.0	3.0	2.5	0.95	0.95	0.95

Note: E_1 and E_2 are in-plane moduli, E_3 is normal modulus, G_{12} is normal shear modulus, G_{23} and G_{13} are in-plane shear moduli, ν_{12} is in-plane Poisson's ratio, and ν_{23} and ν_{13} are normal Poisson's ratios. S_c is shear strength, X_t is in-plane tensile strength, Y_t is normal tensile strength, Y_c is normal compressive strength, S_n is general tensile strength, S_{yz} and S_{xz} are normal shear strengths.

The elastic-plastic material model suitable for the strain rate is selected for the 3D fabric composite plate. Its equation is shown in Eq. (4.3), and the relevant material parameters (Chen *et al.*, 2019) are shown in Table 4

$$\sigma = k\varepsilon^m \dot{\varepsilon}^n \quad (4.3)$$

where σ is the yield stress, ε is the effective plastic strain, and $\dot{\varepsilon}$ is the effective total strain rate. k , m and n are constants relative to the plastic strain.

Table 4. Material parameters of the UHMWPE 3D fabric plate

ρ [g/cm ³]	E [GPa]	ν	k	m	n
0.94	12.5	0.14	350	1.5	2

4.3. Verification of numerical simulation method

In order to verify the correctness of the numerical method, four kinds of composite target plates are simulated. Figure 10 takes structure I and IV as examples to compare the test mode and numerical mode of different failure modes. Table 5 shows the experimental and numerical results of the four structures.

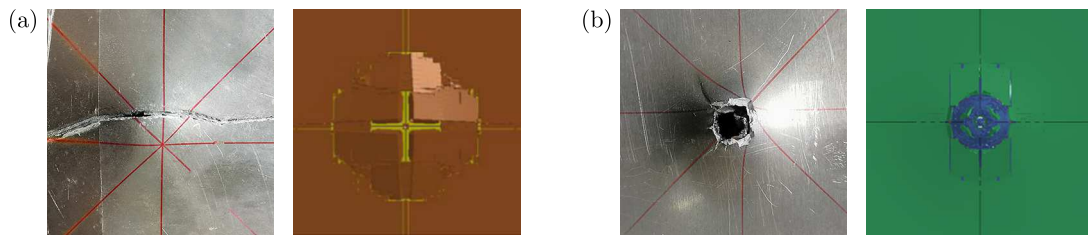


Fig. 10. Failure modes of the penetration test and numerical simulation: (a) structure I back plate, (b) structure IV back plate

Table 5. Comparison of numerical simulation and test results

Structure of target plates	Initial velocity [m/s]	Test residual velocity [m/s]	Simulated residual velocity [m/s]	Error [%]
I	861.71	0	0	–
II	859.63	286.14	259.27	–9.39
III	855.48	0	0	–
IV	856.81	412.91	376.43	–8.83

From the numerical simulation, it can be seen that the simulated failure mode of the projectile penetrating the composite target plate is basically consistent with the test. Comparing the residual velocity of the test and simulation, the absolute error is within 10%. This is due to the error caused by the macro modeling used in UHMWPE fiberboard, which makes the simulation residual velocity decrease, but it can still be explained by the numerical simulation, which has a good accuracy, indicating that the numerical calculation method is validated effectively.

5. Failure mechanism and performance analysis

5.1. Analysis of the anti-penetration failure mechanism

Since structure I has the best anti-penetration performance in the test, only structure I is further analyzed. In the simulation, the projectile velocity is increased so that it is able to

penetrate the target plate, which facilitates the analysis of the whole process. Figure 11 shows the destruction process of the projectile body penetrating structure I at a velocity of 1100 m/s.

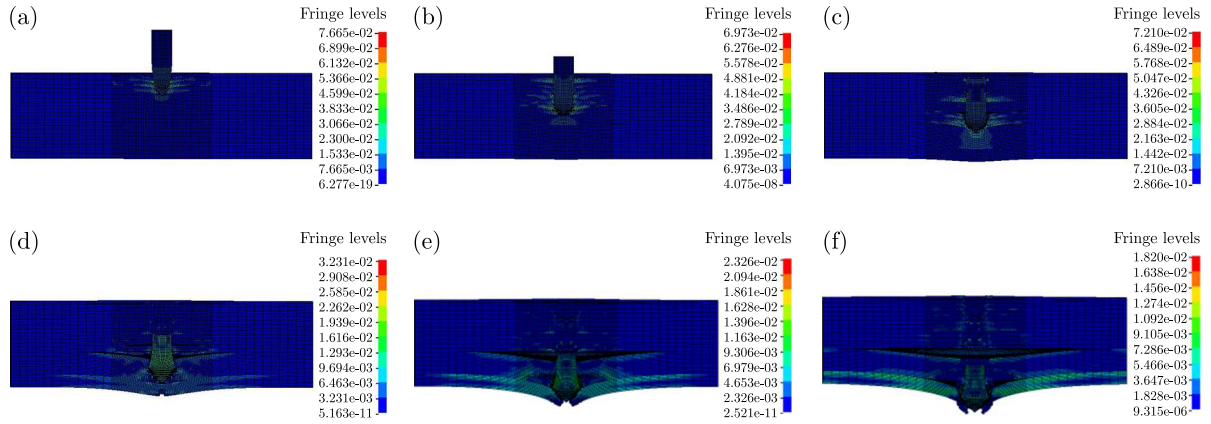


Fig. 11. Damage process of projectile penetration structure I: (a) $t = 12 \mu\text{s}$, (b) $t = 20 \mu\text{s}$, (c) $t = 30 \mu\text{s}$, (d) $t = 45 \mu\text{s}$, (e) $t = 60 \mu\text{s}$, (f) $t = 70 \mu\text{s}$

When the time t is shorter than $20 \mu\text{s}$ and the high-speed projectile penetrates through the front panel and part of the fiber laminar plates, the failure mode of the target plate is mainly shear failure, which generates a compression wave propagating along the thickness direction and the shear wave propagating along the in-plane direction with the impact point as the center. The compression wave causes local compression deformation in the contact area of the projectile and target. The in-plane shear wave causes a large velocity difference between the contact and non-contact regions of the projectile and target, and the fiber layer begins to undergo a shear failure. At this time, the pressure on the fiber layer along the thickness gradually increases from 418 MPa near the panel to 557 MPa and reaches the maximum pressure of 627 MPa near the core. The unidirectional arrangement of the fibers of UD laminates is conducive to the rapid expansion of the shockwave generated instantly by the projectile, and there is no doubt that the fibers are broken due to superposition of the shockwave and reflected wave at the interleaving point, so as to preliminarily consume the kinetic energy of the projectile and erode the projectile. At this point, the UD cloth fiber is subjected to 209 MPa of pressure near the core. When the time t is 20-30 μs , the projectile penetrates into the remaining fiber laminates. At this time, due to the upsetting deformation of the projectile, the fiber laminates are not only sheared, but also subjected to a certain tensile force in the transverse direction. At this time, the pressure on the remaining fiber laminates gradually drops to 360 MPa. However, the 3D fabric and aluminum alloy plate placed on the back provide strong support, and no large deflection occurs on the back of the fiber laminates. Most of the generated energy is absorbed by the interlocking 3D fabric and the energy-absorbing matrix filled in the pores, so that the kinetic energy of the projectile body is rapidly consumed, the pressure on the core is reduced to 216 MPa. When $t = 45 \mu\text{s}$, the projectile body penetrates the fiber laminates and begins to penetrate the 3D fabric plates. At this time, a part of the core is basically abrasive. The fibers of the 3D orthogonal structure pull with each other, which brings great resistance to the advance of the projectile body, and the fracture of the fiber bundles causes kinetic energy of the projectile to be consumed further. At this time, the pressure on the three-dimensional orthogonal fabric and core comes to the minimum value of 161 MPa and 193 MPa. When time $t = 70 \mu\text{s}$, the projectile body impinges the rear aluminum alloy plate and penetrates out, and the residual velocity of the projectile body is 452 m/s.

5.2. Influence of the thickness ratio of 3D fabric on anti-penetration performance

In order to study the influence of different thickness ratios of the 3D fabric on the anti-penetration performance of structure I and obtain the optimal structure proportion, in this Section, the total thickness of the core layer and the thickness of the front and rear panels are kept unchanged. The 3D fabric thickness ratio is shown as

$$\eta = \frac{t_s}{t_c} \cdot 100\% \quad (5.1)$$

where η represents the 3D fabric thickness ratio, t_s represents the thickness of the 3D fabric plate, t_c represents the overall thickness of the core layer.

According to the failure mechanism of the upper segment, the UD laminates should still occupy a large proportion in the core structure, otherwise it is not conducive to the initial resistance to projectile intrusion. Nine kinds of composite structures with different proportions of 3D fabrics are selected for simulation and multiple structures are selected within 50%. Among them, two categories of structures with a single core material are selected for comparison, as shown in Table 6. In order to fully reflect the protective performance of different structures, the projectile velocity should not be set too high or too low. It is suitable to set the initial velocity of the projectile at 1100 m/s by calculation.

Table 6. Composite target plate with different 3D fabric thickness ratios

Structure number	Thickness of front panel [mm]	Thickness of laminates [mm]	3D fabric plate thickness [mm]	Thickness of rear panel [mm]	Total thickness [mm]	Thickness ratio η [%]
1	1	28	0	5	34	0
2		24.5	3.5			12.5
3		21	7			25
4		19	9			32.14
5		17.5	10.5			37.5
6		16	12			42.86
7		14	14			50
8		7	21			75
9		0	28			100

Figure 12 shows the numerical calculation results. According to Fig. 12a, it can be found that the velocity of the projectile body changes with time in the same trend, which gradually decreases without great fluctuation. It can be seen from Fig. 12b that with an increase of the 3D fabric thickness ratio, the residual velocity of the projectile body increases first, then decreases, then increases and decreases again. The minimum residual velocity of the projectile penetrating No. 4 structure is 410.7 m/s.

Because of the density difference between UD laminates and 3D fabrics, the structure quality of different numbers is not exactly the same. Therefore, the energy absorption characteristics of different structures are characterized by the energy absorption coefficient (EAC), which is the ratio of energy absorbed to the mass of the target plate when the projectile penetrates the target plate (Tang *et al.*, 2002), defined as follows

$$EAC = \left(\frac{1}{2}m_p v_i^2 - \frac{1}{2}m_q v_r^2 \right) \frac{1}{M} \quad (5.2)$$

where m_p and m_q are the original mass and residual mass of the projectile body respectively, v_i and v_r are the initial velocity and residual velocity of the projectile body respectively, and M is mass of the target plate.

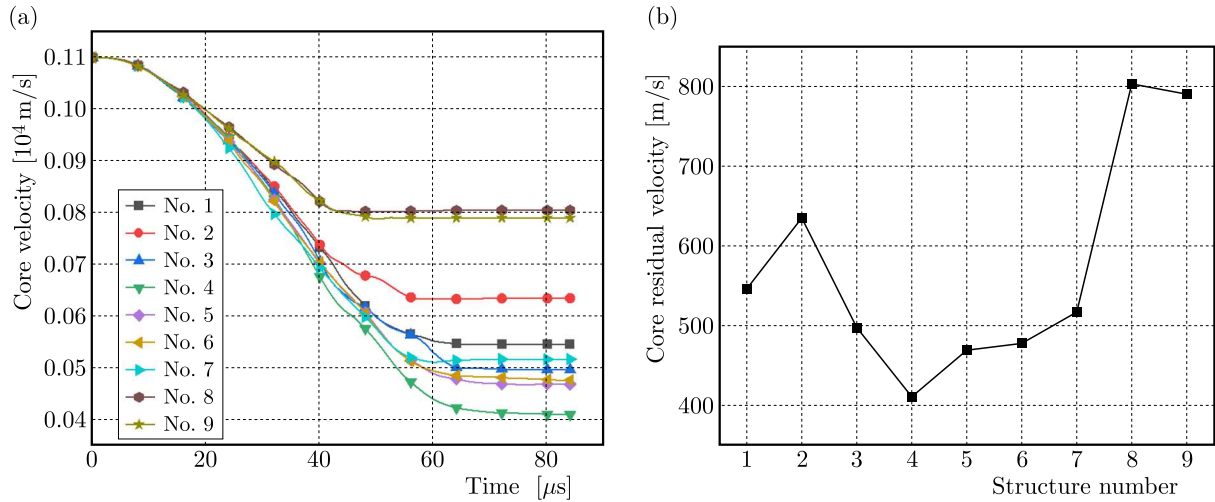


Fig. 12. Numerical simulation results: (a) time history curve of projectile velocity, (b) relation curve between the structure form and residual velocity

The *EAC* of the structure and its related parameters are shown in Table 7, where m_p is 8.4 g and not listed in the table. The relationship between the 3D fabric thickness ratio and *EAC* of different numbered structures is shown in Fig. 13.

Table 7. Structural *EAC* and its related parameters

Structure number	Thickness ratio η [%]	Initial velocity [m/s]	Residual velocity [m/s]	Residual mass of projectile m_q [g]	The mass of target plates M [g]	<i>EAC</i> [J/kg]
1	0		546.2	7.72	998.19	3937.56
2	12.5		634.8	7.60	993.63	3573.47
3	25		497.3	7.56	989.06	4193.05
4	32.14		410.7	7.60	987.04	4499.35
5	37.5	1100	469.1	7.36	985.84	4333.56
6	42.86		477.3	7.52	983.95	4294.34
7	50		517.4	7.60	982.05	4139.03
8	75		803.1	8.04	975.94	2550.59
9	100		790.3	8.20	969.70	2600.03

According to Fig. 13a, No. 4 structure has the highest *EAC*, which is 14.27% higher than that of No. 1 only using UD laminates as the core material, and is 73.05% higher than that of No. 9 only using 3D fabric as the core material. The *EAC* of No. 8 and 9 structures is much less than that of other structures. The reason is that the proportion of the 3D fabric is too high, which leads to the existence of a large number of nodes between 3D orthogonal structures. The fibers at these nodes are prone to fracture under superposition of the shock and reflected waves, which reduces the local impact resistance. According to Fig. 13b, as the 3D fabric thickness ratio increases, the *EAC* decreases first, then increases, then decreases and increases again. Equation (5.3) can be obtained by fitting data points

$$EAC = 3931.9 - 11709\eta + 101174\eta^2 - 260207.3\eta^3 + 253721.2\eta^4 - 84312.2\eta^5 \quad (5.3)$$

where *EAC* represents the energy absorption coefficient and represents the 3D fabric thickness ratio.

In the figure, the 3D fabric thickness ratio corresponding to the maximum point of *EAC* is 32.14%. Therefore, for the composite structure designed in this paper, the optimal proportion of

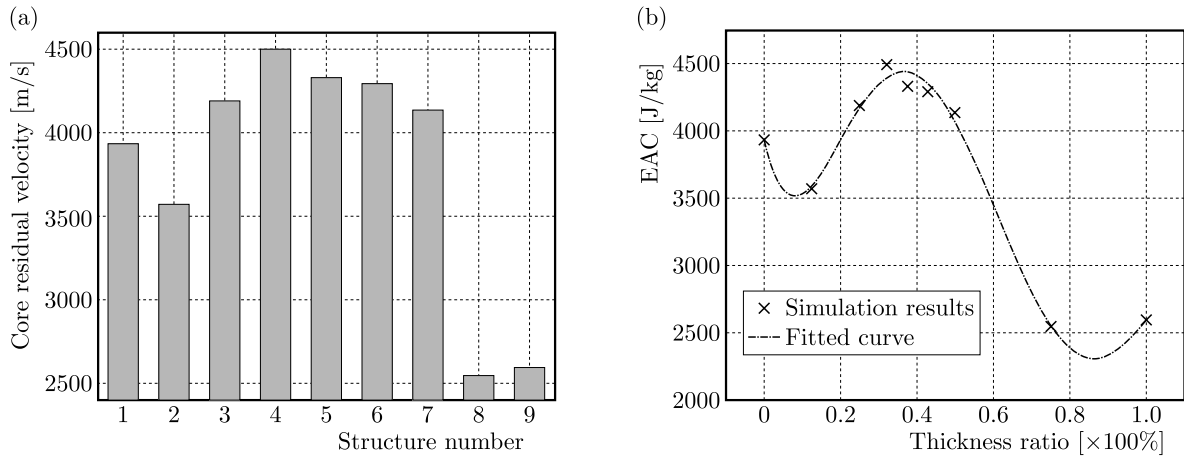


Fig. 13. (a) The relationship between EAC of different structures, (b) relationship between 3D fabric thickness ratio and EAC

the 3D fabric is 25%-37.5%. If considering the requirements of practical engineering lightweight, the 3D fabric thickness ratio is 30%-35% for a better choice.

6. Conclusions

In this paper, a UD/3D orthogonal woven fabric composite reinforced structure is designed based on the UHMWPE fiber material, and penetration tests are carried out on target plates with various reinforced structure forms by using a 7.62 mm steel core projectile. Combined with numerical simulations, the main conclusions are as follows:

- If the total thickness of UD laminates is the same, the 20 mm UD laminates have better penetration resistance than the four 5 mm UD laminates. The less number of UD laminates, the better anti-penetration performance of the composite reinforced structure.
- From analysis of the failure mechanism it occurs that the 3D orthogonal woven fabric has the advantage of spatial integrity, and can effectively resist deformation of UD laminates when placed behind the UD laminates together with an aluminum alloy plate. The fibers pull with each other, which can hinder the advance of the projectile. The fracture of a fiber bundle can enhance consumption of kinetic energy of the projectile.
- In order to ensure the protection capability and take the requirements of lightweight into account, in the structure with a core thickness of 28 mm, the 3D fabric thickness ratio can be controlled between 30% and 35%.

Acknowledgments

This research was supported by the National Natural Science Foundation of China (No. 52301373), the Young Elite Scientists Sponsorship Program by CAST (2022QNRC001), the Natural Science Foundation of Jiangsu Higher Education Institutions of China (No. 22KJB580005).

References

1. CHEN L., DU T., XIAO X., ET AL., 2019, Experimental and numerical simulation of 7075 aluminum target impacted with ogival-nosed projectiles, *Ordnance Materials Science and Engineering*, **42**, 5, 27-32
2. DENG Y., YUAN J., XU J., 2018, Effect of impact angle of rigid oval projectile on penetration characteristics of braided composite laminates, *Journal of Composite Materials*, **35**, 8

3. HU M., SUN B., GU B., 2021, Microstructure modeling multiple transverse impact damages of 3D braided composite based on thermo-mechanical coupling approach, *Composites: Part B: Engineering*, **214**
4. JOHNSON G.R., COOK W.H., 1983, A constitutive model and data for metals subjected to large strains, high strain rates and high temperature, *Proceeding of the 7th International Symposium on Ballistics*, Hague, Netherlands: International Ballistics Committee, 541-547
5. LIANG J., FANG G., 2014, *Mechanical Properties Analysis Method of Three-Dimensional Braided Composites*, Harbin: Harbin University of Technology Press
6. LIU L., 2020, *Research on Anti-Penetration Performance of Ship Protection Module Based on Fiber Reinforcement*, Jiangsu University of Science and Technology
7. QU K.F., WU C.Q., LIU J., YAO Y., DENG Y., YI C., 2020, Ballistic performance of multi-layered aluminium and UHMWPE fibre laminate targets subjected to hypervelocity impact by tungsten alloy ball, *Composite Structures*, **253**
8. SONG M., XUAN H., HE Z., ET AL., 2020, A review of research on 3D braided – woven composite casing containment, *Journal of Mechanical Engineering*, **8**, 31-35+40
9. SUN B., LIU Y., GU B., 2009, A unit cell approach of finite element calculation of ballistic impact damage of 3D orthogonal woven composite, *Composites: Part B: Engineering*, **40**, 6, 552-560
10. TAN H., XU S., HUANG X., ET AL. 2018, Impact damage simulation and experimental verification of 3D four-way braided composite macro-finite element model, *Journal of Composites*, **35**, 5, 1139-1148
11. TANG D., ZHOU B., ZHOU Z., 2002, Experimental study on energy absorption characteristics of steel tube under lateral explosion shock wave loading, *Explosion and Impact*, **22**, 2, 41-46
12. WALTER T.R., SUBHASH G., SANKAR B.V., YEN C.F., 2009, Damage modes in 3D glass fiber epoxy woven composites under high rate of impact loading, *Composites: Part B*, **40**, 584-589
13. WU L., WANG W., JIANG Q., XIANG C., LOU C.-W., 2019, Mechanical characterization and impact damage assessment of hybrid three-dimensional five-directional composites, *Journal of Polymers*, **11**, 9
14. XIONG Z., LIU X., ZHANG Z., ET AL., 2016, Preliminary study on three-dimensional knitted fabric and its engineering protection application, *Journal of Natural Science of Xiangtan University*, **40**, 5, 65-70
15. YOU-ZHI L., GUO-XIN Z., YUE-MING Z., 2008, Study on concrete moisture and drying shrinkage based on mesoscopical damage model, *Engineering Mechanics*, **25**, 7, 196-201

Manuscript received March 7, 2023; accepted for print June 14, 2023